

Journal of Materials Chemistry C

Accepted Manuscript



This is an *Accepted Manuscript*, which has been through the Royal Society of Chemistry peer review process and has been accepted for publication.

Accepted Manuscripts are published online shortly after acceptance, before technical editing, formatting and proof reading. Using this free service, authors can make their results available to the community, in citable form, before we publish the edited article. We will replace this *Accepted Manuscript* with the edited and formatted *Advance Article* as soon as it is available.

You can find more information about *Accepted Manuscripts* in the [Information for Authors](#).

Please note that technical editing may introduce minor changes to the text and/or graphics, which may alter content. The journal's standard [Terms & Conditions](#) and the [Ethical guidelines](#) still apply. In no event shall the Royal Society of Chemistry be held responsible for any errors or omissions in this *Accepted Manuscript* or any consequences arising from the use of any information it contains.

ARTICLE

Roles of oxygen Frenkel pair in the photoluminescence of Bi³⁺-doped Y₂O₃: Computational predictions and experimental verifications

Cite this: DOI: 10.1039/x0xx00000x

Received 00th January 2012,
Accepted 00th January 2012

DOI: 10.1039/x0xx00000x

www.rsc.org/

Heechae Choi^a, So Hye Cho^b, Sovann Khan^b, Kwang-Ryeol Lee^a and Seungchul Kim^{a*}

Bi³⁺ as a dopant in wide-band-gap yttria (Y₂O₃) has been used as a green light emission center or a sensitizer of co-doped rare earth elements. Because the photoluminescence (PL) properties of Y₂O₃:Bi³⁺ vary remarkably according to heat treatments, the roles of point defects have been an open question. Using first-principles calculations and thermodynamic modeling, we have thoroughly investigated the formation of point defects in Y₂O₃:Bi³⁺ at varying oxygen partial pressures and temperatures, as well as their roles in the PL. The photoabsorption energies of the Bi³⁺ dopant were predicted to be 3.1 eV and 3.4 eV for doping at the S₆ and the C₂ sites, respectively, values that are in good agreement with the experimental values. It was predicted that an oxygen interstitial (O_i) and an oxygen vacancy (V_O) are the dominant defects of Y₂O₃:Bi³⁺ at ambient pressure and an annealing temperature of 1300 K (3.19 × 10¹⁶ cm⁻³ for 1% Bi doping), and the concentrations of these defects in doped Y₂O₃ are approximately two orders of magnitude higher than them in undoped Y₂O₃. The defect V_O²⁺ in Y₂O₃:Bi³⁺ was predicted to reduce the intensity of PL from Bi³⁺ at both S₆ and C₂ sites. We verify our computational predictions from our experiments that the stronger PL of both 410 and 500 nm wavelengths was measured for the samples annealed at higher oxygen partial pressure.

Introduction

Transparent bixbyite yttria (Y₂O₃) has been widely used as a host material for trivalent rare earth (RE) dopants, or *activators*, which emit photons in the visible light or the near-infrared (NIR) ranges [1-5]. Its wide band gap (5.5 eV) and low phonon vibrations make yttria a suitable host material for a wide emission range of phosphors. For instances, Eu³⁺-co-doped yttria is used as the best quality material for producing a red light emitting diode (LED), and Yb³⁺-co-doped yttria emits at NIR wavelengths [5-6].

Bi³⁺-doped Y₂O₃ (Y₂O₃:Bi³⁺) has been suggested as a green light (500 nm) emission source, or a sensitizer, to increase the PL intensity from co-doped RE activators [6-12]. The green light emission or sensitization of Bi³⁺ occurs when photons are absorbed by Bi³⁺ at Y-sites, by the 6s² → 6s6p transition, followed by a sequential emission or energy transfer to the activators by the 6s6p → 6s² transition of Bi³⁺ [6-10]. Bi³⁺ absorbs two ranges of wavelengths, 325-346 nm and 370-378 nm, at two nonequivalent sites of yttrium, S₆ and C₂ [7-10]. The

S₆ and the C₂ sites are known to emit at 410 and 500 nm, photons, respectively.

The RE activators in Bi³⁺-doped yttria efficiently absorb photons mostly at 500 nm, which are emitted from the Bi³⁺ at the C₂ site [7-10]. For a higher efficiency of energy conversion in a Bi³⁺-sensitized phosphor, the host lattice should have high crystallinity so that the emission peak from Bi³⁺ at the C₂ site becomes sharp and intense. In addition, the sensitizer-activator distance should be closer because the energy transfer efficiency η_{eff} follows the relation, $\eta_{\text{eff}} \propto 1/R_{\text{SA}}^6$, where R_{SA} is the sensitizer-activator distance. Therefore, the PL intensity increases with the doping concentration of the RE activator up to a certain limit.

Recently, combustion techniques and colloidal methods have been used to synthesize yttria nanophosphors [11-13]. These methods are followed by high-temperature annealing (~1300 K) for increasing the crystallinity and removing the radicals. For Y₂O₃:Bi³⁺ synthesis, the former method is more frequently

employed. The optimized Bi mole percentage that gives the best PL intensity and peak broadness by Bi^{3+} at the S_6 and the C_2 sites is heavily influenced by several fabrication conditions [10–14]. For example, Jacobsohn *et al.* reported that the type of combustion fuel affects the PL properties; in particular, they showed that urea as the fuel gives the best peak sharpness with equal intensities from Bi^{3+} at the S_6 and the C_2 sites [14]. The work of Huang [10], which used longer annealing time, however, showed a weaker and a broader PL peak from Bi^{3+} at the C_2 site than that from the S_6 site, despite the use of identical chemical starting materials and fuels as for the study of Jacobsohn.

The origins of this discrepancy in the optical properties mostly fall into two cases: the formation of a variety of phases or the introduction of native defects. It is reasonable to exclude the formation of a variety of phases for $\text{Y}_2\text{O}_3:\text{Bi}^{3+}$ synthesis because X-ray diffraction (XRD) measurements demonstrated the uniform bixbyite structure after an annealing process [7–11, 14]. Therefore, native defects and defect doping with H, C or N atoms can exist and influence the optical properties of the crystals, as can be seen in other phosphor materials that have been well-studied theoretically, such as GaN and ZnO [15–19]. However, the conditions of the heat treatments also significantly alter the peak broadness and intensity; hence, the roles of the native defects are important in the $\text{Y}_2\text{O}_3:\text{Bi}^{3+}$ system.

We theoretically investigated the formation of native point defects in $\text{Y}_2\text{O}_3:\text{Bi}^{3+}$ in the experimentally employed conditions for the annealing temperature and the oxygen pressure, as well as their roles in the PL properties. Based on the defect energy levels, we predicted the absorption wavelengths of each defect system. Our defect modeling includes dopant-defect complexes to thoroughly investigate the effects of doped Bi on the energetic stability and the energy levels of point defects. In addition, we prepared $\text{Y}_2\text{O}_3:\text{Bi}^{3+}$ phosphors under oxygen-poor, ambient, and oxygen-rich conditions and compared their PL intensities. The result showed the good agreement between the theoretical predictions and experimental outputs.

Calculation methods

We performed density functional theory (DFT) calculations within the generalized gradient approximation (GGA), with Perdew-Burke-Ernzerhof (PBE) parameterization [25, 26]. We used the VASP software [21], and atomic nuclei and core electrons were described by a projector-augmented wave (PAW) [24]. Kohn-Sham orbitals were expanded with a cutoff energy of 450 eV, and a $3 \times 3 \times 3$ equally spaced k -point grid was used for the Brillouin zone sampling. A Hubbard U approximation ($U_{5d} = 6$ eV) term [27] was included to correct the splitting of the $5-d$ orbital of yttrium, and the spin-orbit coupling (SOC) was included for the correct description of the bismuth orbitals. With the SOC term, our calculations agreed well with the experimental observations of the $6s$ and the $6p$ states of bismuth [6–12]. In the formation energy calculations, the experimental binding energy of an oxygen molecule, 2.56 eV/atom, was employed instead of the GGA value, which is known to significantly overestimate the bonding energy of O_2 molecule

[28]. The yttria unit cell contains 32 yttrium atoms (8 at the S_6 sites and 24 at the C_2 sites) and 48 oxygen atoms, as presented in Fig. 1. The cell volume and all atoms were fully relaxed. The Bi^{3+} -doped Y_2O_3 was modeled with the incorporation of one Bi^{3+} ion at an interstitial site (Bi_i) or at two yttrium sites, S_6 and C_2 .

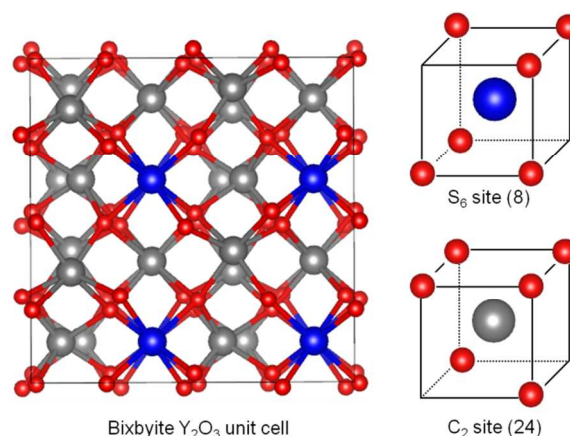


Fig. 1. Atomic model of the bixbyite structure. Red spheres are O atoms, and blue and grey spheres are Y atoms at the S_6 and the C_2 sites, respectively. The numbers in the parentheses are the number of the S_6 and the C_2 sites in the primitive unit cell.

Results and Discussions

a. Formation energies and electronic structures of Y_2O_3 and $\text{Y}_2\text{O}_3:\text{Bi}$

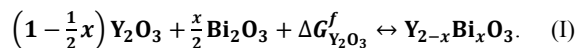
The formation energy of yttria ($\Delta E_{\text{Y}_2\text{O}_3}^f$) was calculated using the equation,

$$\Delta E_{\text{Y}_2\text{O}_3}^f = E_{\text{Y}_2\text{O}_3} - 2E_{\text{Y}} - \frac{3}{2}E_{\text{O}_2}, \quad (1)$$

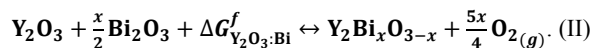
where $E_{\text{Y}_2\text{O}_3}$, E_{Y} and E_{O_2} are the total energies of the yttria crystal, solid yttrium, and an isolated oxygen molecule, respectively. The formation energy ($\Delta E_{\text{Y}_2\text{O}_3}^f$), the lattice constant and the band gap of yttria are presented in Table I, along with a comparison to the values from a previous DFT study [23] performed using the GGA functional of Perdew-Wang (PW91) [21] and an experimental study [29]. The formation energy and the lattice constant from the PBE calculations are very close to the experimental values, as is shown in Table I. The band gap was underestimated in the PBE calculations, whereas it was corrected to nearly the experimental value by inclusion of U ($U_{5d} = 6$ eV). The SOC term gives negligible changes in the band gap of yttria.

The free energy of Bi-doping was calculated using the chemical reactions below (reactions I, II and III). Temperatures of 800 and 1300 K were considered because combustion and annealing were performed at these temperatures in many reported experiments [7–10]. The solid and liquid phases of bismuth oxide (Bi_2O_3) were considered as references for the bismuth chemical potential for 800 and 1300 K, respectively, because the melting point is 1100 K [11, 14].

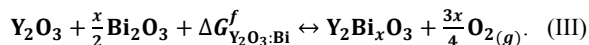
Substitution of Y:



Substitution of O (anti-site):



Bi interstitial:



The Bi-doping energy ($\Delta G_{Y_2O_3:Bi}^f$) is the change in the free energy by Bi-doping per Bi atom. In our calculations of $\Delta G_{Y_2O_3:Bi}^f$, the thermal energies of the solids ($Y_2O_3:Bi$, Y_2O_3 and Bi_2O_3) were ignored because their contributions to $\Delta G_{Y_2O_3:Bi}^f$ would be largely cancelled out. Hence, the Gibbs free energies can be replaced by the calculated total energies of $Y_2O_3:Bi$ and Y_2O_3 . The calculated $\Delta G_{Y_2O_3:Bi}^f$ under extremely oxidizing and reducing conditions at 298 K are listed in Table II. The upper limit of the oxygen chemical potential, which is under extremely oxidizing conditions, is given by:

$$\mu_O \leq \mu_O^0 = \frac{1}{2} E_{O_2}. \quad (2)$$

The lower limit can be defined when yttria is decomposed into solid yttrium and oxygen gas. Thus, $\mu_Y = \mu_Y^0 = E_Y$ under extremely reducing conditions, where E_Y is the total energy of yttrium in the solid phase. The chemical potential of oxygen was calculated using the thermodynamic equation for ideal gases and the chemical potential at standard temperature and pressure. As the reference point, μ_O^0 is used as the zero point:

$$\Delta\mu_O = \mu_O - \mu_O^0. \quad (3)$$

The oxygen chemical potential was expressed as:

$$\Delta\mu_O(T, P_{O_2}) = \frac{1}{2} \left\{ \tilde{\mu}_{O_2}(T, P^0) + k_B T \ln\left(\frac{P_{O_2}}{P^0}\right) \right\}, \quad (4)$$

where $\tilde{\mu}_{O_2}(T, P^0)$ is the O_2 chemical potential at standard pressure (P^0) and temperature T [30].

The Bi-doping energy ($\Delta G_{Y_2O_3:Bi}^f$) of the reactions considered are in Table II and are plotted in Fig. 2 for the two representative temperatures of 800 K and 1300 K with varying oxygen pressures. The experimental heat of fusion of Bi_2O_3 , 6.8 kcal/mole (0.30 eV/f.u.) [31], which is higher than the melting temperature of Bi_2O_3 , was added to the formation energy for calculations at 1300 K. Our calculations show that substitutional Bi^{3+} doping at the S_6 site is the more favorable, than at the C_2 site by the energy difference of 0.08eV. The preference of Bi^{3+} at S_6 is well consistent with the tendency found in the Stanek's simulation work using Buckingham potentials: a dopant with larger ionic radius than host cation favors the S_6 site of an oxide in bixbyite structure [32]. Bi as an interstitial or an anti-site defect is very high in energy at atmospheric conditions. Obeying the Boltzmann factor,

$N_{Bi_{C_2}}/N_{Bi_{S_6}} = \frac{N_{C_2}}{N_{S_6}} \exp\left[\frac{E_{Bi_{C_2}} - E_{Bi_{S_6}}}{k_B T}\right]$, the Bi^{3+} populations at the S_6 and the C_2 sites are in the ratio of 1:0.94 at 800 K, and 1:1.47 at 1300 K. At higher temperature, the pre-exponential factor ($\frac{N_{C_2}}{N_{S_6}} = 3$) becomes more important than the energy difference, such that the population at the C_2 sites becomes larger. The tendency for an increase in the amount of Bi^{3+} at the C_2 sites as the temperature increases is consistent with the tendency for an increase in the amount of Bi at the C_2 sites when a fuel with a large heat of combustion was used. [14]

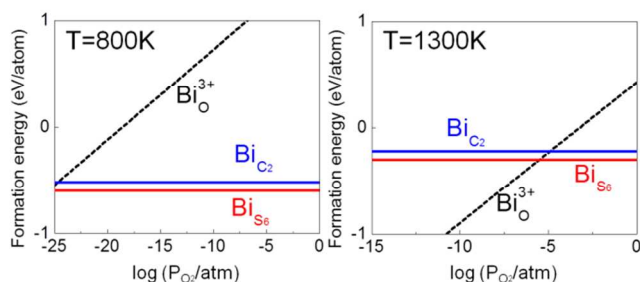
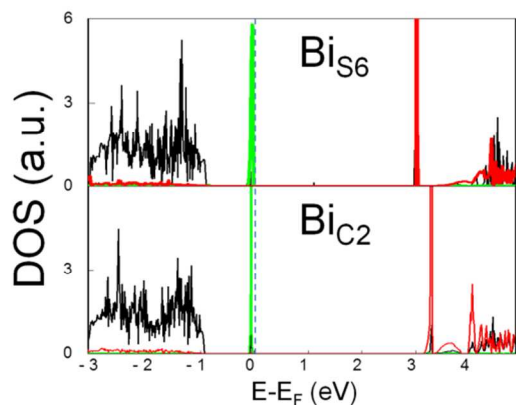
	ΔE^f (eV/f.u.)	Lattice constant (Å)	Band gap (eV)
PW (Ref. 21)	-19.41	10.700	4.1
PBE (This work)	-20.47	10.605	4.6
PBE+U (This work)	-	-	5.3
Experiment (Ref.22)	-20.29	10.604	5.5

Table I. Calculated and experimental formation energy (ΔE^f) per formula unit, lattice constant, and band gap of Y_2O_3 .

Doping Type	Net Charge (e)	Bi-doping energy (eV/Bi-atom)		Lattice Constant (Å)
		$\mu_O = \mu_O^0$	$\mu_Y = \mu_Y^0$	
Bi_{S_6}	0	-0.60	-0.60	10.613
Bi_{C_2}	0	-0.52	-0.52	10.612
Bi_{iO}	0	14.04	3.04	10.668
	+1	9.78	-1.22	10.648
	+2	6.29	-4.71	10.629
	+3	2.38	-8.62	10.595
Bi_i	0	13.44	6.84	10.678
	+1	11.36	4.76	10.650
	+2	10.54	3.94	10.629

+3 9.62 3.02 10.610

Table II. Bi doping energies at 298 K and the corresponding lattice constants.

Fig. 2. The calculated Bi doping energy ($\Delta G_{Y_2O_3:Bi}^f$) as a function of P_{O_2} at 800 K and 1300 K. Anti-site (Bi_O) doping becomes dominant below $P_{O_2} = 4.0 \times 10^{-26}$ atm at 800 K and $P_{O_2} = 2.5 \times 10^{-6}$ atm at 1300 K.Fig. 3. Electron density of states of Bi-doped Y_2O_3 . Green and red curves are PDOS of Bi $6s$ and $6p$, and black curve is the total DOS. The black curves were normalized by the number of atoms.

The localized $6s$ - and $6p$ -orbitals of Bi^{3+} appear very clearly in the electron density of states (DOS) in Fig. 3. The separation of the $6s$ - and the $6p$ -orbitals was not described well without the SOC. The Bi^{3+} at both the S_6 and the C_2 sites has sharply localized $6s$ - (occupied) and $6p$ - (unoccupied) orbitals within the band gap of the yttria host. The calculated energy distances between the in-gap $6s$ - and $6p$ -orbitals are 3.10 (400 nm) and 3.42 eV (362 nm) for the S_6 and the C_2 sites, respectively. The wavelengths of excitation correspond to the $6s$ - $6p$ separations, which lead to the $^1S_0 \rightarrow ^1P_1$ transitions being slightly longer than the experimental measurements, 378 nm and 325 nm [7-8, 10, 14]. One common method to correct the energy levels for an underestimated band gap is to rigidly shift the occupied states and the unoccupied states as much as the gap

under estimation, while fixing the level intervals between the occupied states and between the unoccupied states. With this method, the corrected $^1S_0 \rightarrow ^1P_1$ transition wavelengths of Bi^{3+} at the S_6 and the C_2 sites are 376 and 342 nm, respectively, which agrees very well with the experiments.

Defect	Charge on defect (e)	Formation energy (eV)	
		$\mu_Y = \mu_Y^0$	$\mu_O = \mu_O^0$
V_O	0	0.62	7.44
	+1	-4.05	2.77
	+2	-7.76	-0.94
V_{S6}	0	13.59	3.35
	-1	14.58	4.34
	-2	15.88	5.64
	-3	17.31	7.07
	0	13.71	3.47
V_{C2}	-1	14.80	4.56
	-2	16.21	5.97
	-3	19.34	9.10
Pure Y_2O_3	O_i 0	7.70	0.88
	-1	9.33	2.51
	-2	11.19	4.37
Y_i	0	3.92	14.16
	+1	-0.70	9.54
	+2	-5.36	4.88
O_{C2}	+3	-8.95	1.19
	0	18.24	1.16
	-1	20.04	2.98
Y_O	-2	23.12	6.06
	0	5.86	22.92
	+1	0.46	17.52
V_O-Bi_{S6}	+2	-4.68	12.38
	+3	-9.39	7.67
	0	-1.16	5.55
V_O-Bi_{C2}	+1	-4.88	1.83
	+2	-8.76	-2.05
$Y_2O_3:Bi$	0	-0.67	6.04
	+1	-4.58	2.13
	+2	-5.11	-1.60
O_i-Bi_{S6}	0	6.57	-0.14
	-1	8.54	1.83
O_i-Bi_{C2}	-2	11.20	4.49
	0	6.46	-0.25
O_i-Bi_{C2}	-1	8.31	1.60
	-2	10.89	4.18

Table III. Point defect formation energies in bixbyite Y_2O_3 under extremely reducing ($\mu_Y = \mu_Y^0$) and oxidizing ($\mu_O = \mu_O^0$) conditions, the upper limits of eqn. (5) and (6). V_O-Bi_{S6} is an O vacancy in the

vicinity of Bi^{3+} at the S_6 site, and the other notations were made in the same way.

Because the photoexcitation by Bi^{3+} occurs between the states within the band gap of the host material, the sensitized luminescence of

$\text{Y}_2\text{O}_3:\text{Bi}^{3+}\text{-RE}$ does not follow the theoretical scheme of Mott and Gurney [33], in which the electrons and holes recombine at the activator ions. The energy transfer with a 500 nm photon emitted from Bi^{3+} at the C_2 site mainly contributes to the sensitization.

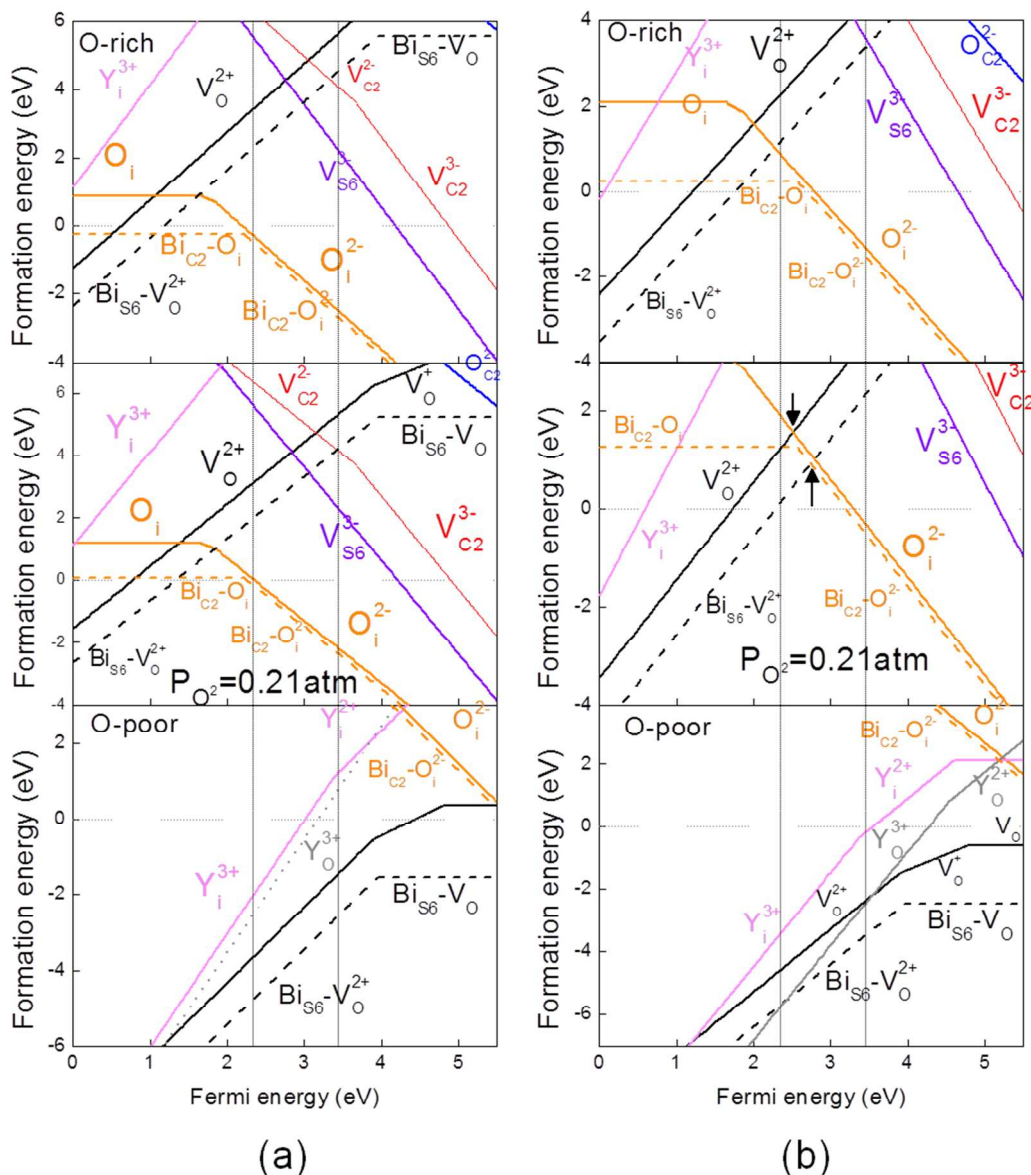


Fig. 4. Defect formation energy for $P_{\text{O}_2} = 0.21$ atm, O-rich and O-poor limits at (a) 300 K and (b) 1300 K, as a function of Fermi level in the gap of yttria. Slopes of each line are the charges of the defects. Solid and dashed lines are the formation energies for pure and Bi^{3+} -doped Y_2O_3 .

b. Defect formations in Y_2O_3 and $\text{Y}_2\text{O}_3:\text{Bi}$

We calculated the point defect formation energies of Y_2O_3 and $\text{Y}_2\text{O}_3:\text{Bi}^{3+}$ within the chemical potential ranges of Y and O, given by:

$$\mu_{\text{Y}}^0 + \frac{1}{2} \Delta E_{\text{Y}_2\text{O}_3}^f < \mu_{\text{Y}} \leq \mu_{\text{Y}}^0 \quad (5)$$

$$\mu_{\text{O}}^0 + \frac{1}{3} \Delta E_{\text{Y}_2\text{O}_3}^f < \mu_{\text{O}} \leq \mu_{\text{O}}^0 \quad (6)$$

We considered the native point defects of pure Y_2O_3 to be oxygen vacancies (V_o), yttrium vacancies at the S_6 (V_{S_6}) and the C_2 (V_{C_2}) sites and interstitial oxygen (O_i) and yttrium (Y_i). In addition, we also included the complexes of each point defect and bismuth at the nearest distance, to investigate the affinity of point defects for the bismuth dopant, which may change the defect concentrations and electronic structures. We also considered the defect to be charged.

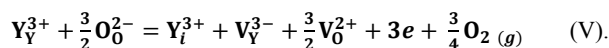
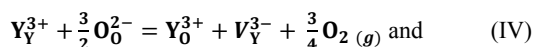
Equation (7) gives the defect formation energies of point defects with a charge q (ΔE_f^q), as a function of the Fermi level, using the equation:

$$\Delta E_f^q(q) = E[D^q] \pm \mu_i - E^0 + q(E_v + \Delta V + \epsilon_F), \quad (7)$$

where $E[D^q]$ is the total energy of the defect-containing Y_2O_3 ($Y_2O_3:Bi^{3+}$) cell with a charge q , E^0 is the total energy of the defect-free Y_2O_3 ($Y_2O_3:Bi^{3+}$), μ_i is the chemical potential of the element i added to (removed from) the Y_2O_3 ($Y_2O_3:Bi^{3+}$) cell to generate a point defect, E_v is the valence band maximum (VBM) of the defect-free Y_2O_3 , ΔV is the shift in the VBM in the defective cell by a point defect, relative to that in the defect-free Y_2O_3 , and ϵ_F is the Fermi level referenced to E_v .

The calculated formation energies of the point defects of yttria under extremely oxidizing ($\mu_O = \mu_O^0$) and reducing ($\mu_Y = \mu_Y^0$) conditions, when the Fermi level is at the VBM, are listed in Table III. Between the two types of interstitial sites in the bixbyite structure, site 8a with six oxygen and six yttrium atoms at its neighbors and site 16c with six oxygen and four yttrium atoms at its neighbors, site 16c is preferred by both the yttrium and the oxygen atoms. We compared the energetic stabilities of the point defects in the pure yttria and the adjacent sites to the doped Bi atom in $Y_2O_3:Bi^{3+}$. Among the point defects considered in this study, only V_O and O_i prefer to be in the vicinity of the doped Bi atom at the S_6 and the C_2 sites, respectively. Other point defects have a higher formation energy than those in the pure yttria.

The pure yttria at room temperature ($T = 300$ K) (Fig. 4(a)) has the same dominant defects under O-rich conditions and at atmospheric oxygen pressure ($P_{O_2} = 0.21$ atm): the V_O^{2+} defect in the p -type region and O_i , O_i^- and O_i^{2-} in the n -type region. In the O-poor limit at 300 K for pure Y_2O_3 , the defects Y_i^{3+} , Y_O^{3+} and V_O^{2+} are competing in the p -type region, and the V_O^{2+} , V_O^+ and V_O defects become the dominant defects as it becomes n -type, following the reaction formula:



At heat treatment temperature and atmosphere ($T = 1300$ K, $P_{O_2} = 0.21$ atm), the dominant point defects in the pure and the Bi-doped yttria are the oxygen Frenkel pair (V_O^{2+} and O_i^{2-}), as Fermi level is pinned at the intersection of the $Bi_{S_6}-V_O^{2+}$ and the $Bi_{C_2}-O_i$ curves. The concentrations of the defect pairs in pure and 1%-Bi doped yttria are $1.31 \times 10^{15} \text{ cm}^{-3}$ and $3.19 \times 10^{16} \text{ cm}^{-3}$, respectively, according to the equation,

$$[V_O^{2+}] = [O_i^{2-}] = \exp\left[\frac{\Delta E_f(q)}{k_B T}\right], \quad (8)$$

where $[V_O^{2+}]$ and $[O_i^{2-}]$ are the concentrations, and $\Delta E_f(q)$ is the defect formation energy of each defect obtained at the pinned Fermi level (Fig. 4(b)).

In O-poor limit at $T = 1300$ K, the Bi-doped Y_2O_3 also has Y_O^{3+} due to the temperature effect. We attribute the lower formation energies of oxygen vacancies in the vicinity of the Bi^{3+} dopant to the longer Bi-O bond lengths than those of Y-O. The bond lengths of Bi-O and Y-O obtained from PBE schemes show same tendency with those from the *ab initio* embedded cluster methods [34]: the bond lengths of Bi-O and Y-O at S_6 are larger than two of those at C_2 site and smaller than the last one (Table IV). The PBE method gives bond lengths and lattice constants, which are closer to the experimental values (See Table I). As is discussed in the next section, much higher concentrations of V_O^{2+} and O_i^{2-} Frenkel defect pairs in $Y_2O_3:Bi^{3+}$ might remarkably change the optical properties of the system during the high temperature treatment.

Cation site	Cation Element	$d1$ (Å)	$d2$ (Å)	$d3$ (Å)
S_6	Y	2.285	-	-
	Bi	2.370	-	-
C_2	Y	2.246	2.263	2.343
	Bi	2.299	2.362	2.445

Table IV. Calculated bond lengths between cations (Y, Bi) and oxygen in Y_2O_3 and $Y_2O_3:Bi^{3+}$. The notation $d1$, $d2$ and $d3$ are the cation-anion distances in sequences.

c. Effects of point defects on the electronic structures and optical properties of Y_2O_3 and $Y_2O_3:Bi$

We present the electron density of states (DOS) for the defect-containing yttria in Fig. 5. The neutral (V_O) and the singly charged oxygen vacancies (V_O^+) in the yttria induce deep donor-like levels. The doubly charged oxygen vacancy (V_O^{2+}) induces a deep unoccupied state in the middle of the yttria band gap. The O_i^{2-} defect induces occupied levels near the VBM, which are filled by oxygen $2p$ electrons. The expected photon energy absorbed by the Y_i^{3+} from the positions of the Fermi level and the induced in-gap states from the calculated DOS is 4-5 eV, which is expected to have an effect on the energy transfer or the emission from the Bi^{3+} dopant. On the other hand, Y_O^{3+} has donor-like states in the gap and also induces the level to coordinate strongly to four yttrium atoms (one S_6 and three C_2 sites). One of the expected photoexcitation energies from the Y_O^{3+} is at approximately 1.2 eV, which is fatal for the NIR emitting phosphor. Note that the discussion for the defects in yttria can be applied to the same type of defects in the $Y_2O_3:Bi^{3+}$ system when the sites are far away from the bismuth atoms.

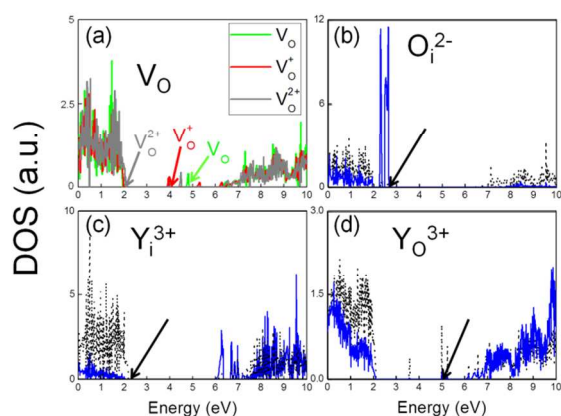


Fig. 5. Electron DOS for defect-containing Y_2O_3 . The black dotted lines are the DOS of the total system containing a point defect, normalized by the number of atoms. The blue solid curves are the DOS of the defect atoms. The arrows point to the highest occupied states.

The energetic stability of the oxygen vacancy and the interstitial defects near the doped Bi^{3+} atom at the S_6 and the C_2 sites was demonstrated in the previous section. In Fig. 6, accordingly, the electron DOS of Bi at the S_6 and the C_2 sites that are altered by the adjacent V_O^{2+} and O_i^{2-} defects are presented. The theoretically predicted photoexcitation energy in Bi at the S_6 site by the $6s^2 \rightarrow 6s6p$ transitions is changed from 3.1 eV to 2.5 and 3.6 eV by the adjacent V_O^{2+} , as can be inferred from the positions of the two split, unoccupied $6p$ levels (Fig. 6(a)). When the oxygen vacancy is neutral, one of the $6p$ levels is occupied. The Bi atom at the C_2 site has the broad peaks of the $6s$ - and the $6p$ -orbitals below the VBM resulting from the strong hybridization with the adjacent O_i^{2-} defect atom. Hence, the photoexcitation peak from the Bi- O_i^{2-} complex is expected to have a broader peak in the higher energy region than for the defect-free case. When the adjacent oxygen interstitial is neutral, the $6s$ orbital is unoccupied, which indicates negligible photoexcitation in Bi^{3+} .

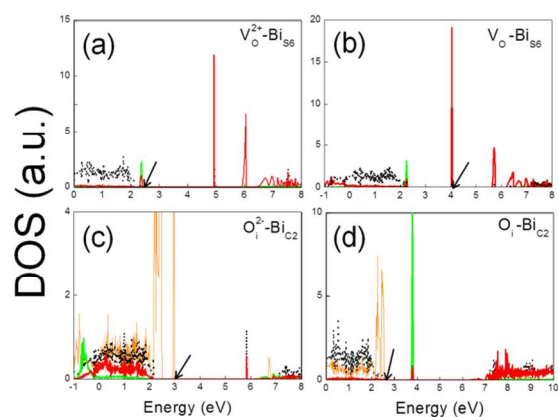


Fig. 6. Electron DOS of defective $\text{Y}_2\text{O}_3:\text{Bi}^{3+}$. The black dotted lines are the DOS of the total system normalized by the number of atoms; green and red solid lines are the DOS of $6s$ and $6p$ orbitals of doped Bi^{3+} ; solid orange line is DOS of the interstitial oxygen.

Because a good phosphor should not absorb the emitted light from the dopants and waste the photon energy, we tested whether the two major defects of O_i^{2-} and V_O^{2+} absorb emitted photons from the bismuth dopants. We found that O_i^{2-} in the vicinity of Bi^{3+} at C_2 site absorbs photon energy of 4.08 eV (304nm), which is much higher energy than emission from Bi^{3+} . On the other hand, V_O^{2+} in the vicinity of S_6 site can absorb the emission from Bi^{3+} at C_2 site such that it degrades the performance of the phosphor. Bi^{3+} at the C_2 site emits around 500 nm wavelength photons [5-10]. As is drawn in Fig. 6, V_O^{2+} absorbs 473 nm and 492 nm photons, which are similar in wavelength to the emitted photon from Bi^{3+} . On the other hand, O_i^{2-} does not absorb such photons (Fig. 6(c)), and thus, an oxygen interstitial will not cause harm to the PL properties of the phosphor.

The dominant point defects of $\text{Y}_2\text{O}_3:\text{Bi}^{3+}$ annealed at high temperature have long been in question. Our DFT calculations predict that the dominant point defects are the Frenkel pair of V_O^{2+} and O_i^{2-} , with concentrations of $3.19 \times 10^{16} \text{ cm}^{-3}$ for 1% Bi doping, which is dense enough to significantly affect the optical properties [35, 36]. From the calculated defect formation energies and the absorption wavelength of defect sites, we found that the Bi^{3+} doping increases the concentration of V_O^{2+} defects which absorb the significant amount of photons emitted not only from Bi^{3+} at the S_6 site, where V_O^{2+} is located, but also from Bi^{3+} at the C_2 site. Thus, we expect that annealing under oxygen-rich conditions is effective for achieving high emission intensity from Bi^{3+} in the Y_2O_3 host, by preventing V_O^{2+} formation. Our prediction is well proven by the experimental results obtained with $\text{Y}_2\text{O}_3:\text{Bi}^{3+}$ phosphors prepared under different environments in the next section.

d. Effect of annealing atmosphere on the photoluminescence of $\text{Y}_2\text{O}_3:\text{Bi}^{3+}$

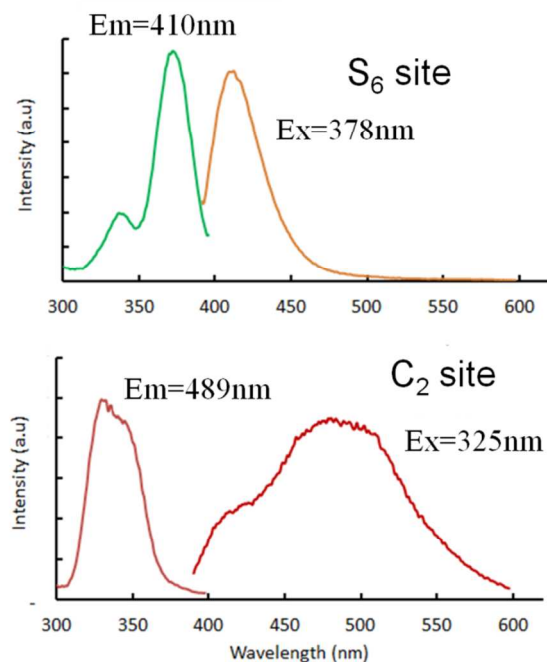


Fig 7. PL and PLE patterns of $\text{Y}_2\text{O}_3:\text{Bi}^{3+}$ prepared under ambient atmosphere.

As it mentioned earlier, several different groups applied the combustion method to obtain $\text{Y}_2\text{O}_3:\text{Bi}^{3+}$ nanophosphors. Jacobsohn *et al.*, in particular, monitored the heat of combustion of different fuels and found that the emission properties of Bi are significantly influenced by fuels [14]. However, the heating atmosphere has not yet been monitored as a variable. Therefore we followed the combustion method reported by Jacobsohn *et al.* to make $\text{Y}_2\text{O}_3:\text{Bi}^{3+}$ and varied the annealing atmosphere to apply our prediction to the real synthetic condition. We prepared 1% Bi-doped $\text{Y}_2\text{O}_3:\text{Bi}^{3+}$ phosphors and annealed them at 1200 °C for 2 h under ambient condition, oxygen-rich (O_2 , >99.9%, 1 atm) and oxygen-poor atmosphere (N_2 , >99.9%, 1 atm), respectively. $\text{Y}_2\text{O}_3:\text{Bi}^{3+}$ prepared under ambient condition showed a very similar PL and PLE patterns as reported by Jacobsohn *et al.* (Fig. 7) [14]. Interestingly, when the annealing atmosphere was changed to oxygen poor, both S_6 and C_2 emission decreased by ~13% at λ_{max} whereas under oxygen rich condition, their emission increased by ~12% (Fig. 8). The increase of PL intensity can be important because the quantum efficiency of nanophosphors is often considered lower than 20% and hence every small increase counts for the improvement.

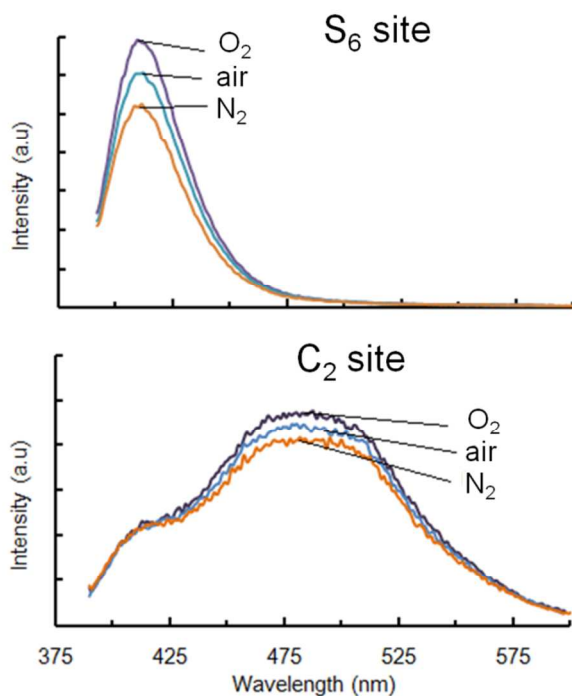


Fig 8. PL of S_6 and C_2 sites of $\text{Y}_2\text{O}_3:\text{Bi}^{3+}$ prepared under ambient, O_2 , and N_2 atmosphere, respectively.

Conclusions

We systematically investigated the formation of point defects in the $\text{Y}_2\text{O}_3:\text{Bi}^{3+}$ system and their effects on the optical properties. We demonstrated that the Bi-doped bixbyite yttria phosphor has a higher defect concentration than the pure matrix. Especially at high temperature (*e.g.*, 1300 K) and at ambient pressure, the Frenkel defect pair of oxygen (V_O and O_i) is dominant in $\text{Y}_2\text{O}_3:\text{Bi}^{3+}$, with concentrations of $3.19 \times 10^{16} \text{ cm}^{-3}$ for 1% Bi doping. The V_O^{2+} becomes the re-absorption center

for the photons emitted from Bi^{3+} at the C_2 site, such that it degrades the efficiency of the green emission or the energy transfer from the Bi dopant to the activator atoms. Our experimental PL measurements agree well with our theoretical prediction. Therefore, we suggest a high-temperature treatment under a high-oxygen partial pressure to achieve high efficiency for $\text{Y}_2\text{O}_3:\text{Bi}^{3+}$ phosphors.

Acknowledgements

We thank the support of the KIST internal projects (Grant No. 2E23891 and 2E24630).

References

1. S. Ray, P. Pramanik, A. Singha, and A. Roy, *J. Appl. Phys.*, 2005, **97**, 094312.
2. V. K. Rai, A. Pandey, and R. Dey, *J. Appl. Phys.* 113 (2013) 083104.
3. X.-L. Liu, P.-X. Zhu, Y.-F. Gao, and R.-H. Jin, *J. Mater. Chem. C* 2013, **1**, 477.
4. R. H. Krishna, B. M. Nagabhushana, H. Nagabhushana, N. S. Murthy, S. C. Sharma, C. Shivakumara, and R. P. S. Chakradhar, *J. Phys. Chem. C* 2013, **117**, 1915.
5. W. Zhu, Y. Wu, A. Leto, J. Du, and G. Pezzotti, *J. Phys. Chem. A* 2013, **117**, 3599.
6. P. Chung, H. Chung, and P. H. Holloway, *J. Vac. Sci. Technol. A* 2007, **25**, 61.
7. L. S. Chi, R. S. Liu, B. J. Lee, *J. Electrochem. Soc.* 2005, **152**, J93.
8. G. Ju, Y. Hu, C. Li, X. Wang, Z. Mu, H. Wu, F. Kang, *J. Lumin.* 2012, **132**, 1853.
9. X.-T. Wei, J.-B. Zhao, Y.-H. Chen, M. Yin, and Y. Li, *Chin. Phys. B* 2010, **19**, 077804.
10. X. Y. Huang, X. H. Ji, and Q. Y. Zhang, *J. Am. Ceram. Soc.* 2011, **94**, 833.
11. J.-L. Yuan, X.-Y. Zeng, J.-T. Zhao, Z.-J. Zhang, H.-H. Chen, and X.-X. Yang, *J. Phys. D: Appl. Phys.* 2008, **41**, 105406.
12. J. J. Kingsley and K. C. Patil, *Mater. Lett.* 1988, **6**, 427.
13. D. Zhao, S. Seo, H. Zhang, B. S. Bae, and W. Qin, *J. Nanosci. Nanotechnol.* 2010, **10**, 2036.
14. L. G. Jacobsohn, M. W. Blair, S. C. Tomga, L. O. Brown, B. L. Bennett, and R. E. Muenchausen, *J. Appl. Phys.* 2008, **104**, 124303.
15. A. Alkauskas, J. L. Lyons, D. Steiauf, and C. G. Van de Walle, *Phys. Rev. Lett.* 2012, **109**, 267401.
16. Q. Yan, A. Janotti, M. Scheffler, and C. G. Van de Walle, *Appl. Phys. Lett.* 2012, **100**, 142110.
17. A. Janotti, and C. G. Van de Walle, 2009. *Rep. Prog. Phys.* 2009, **72**, 126501.
18. J. L. Lyons, A. Janotti, and C. G. Van de Walle, *Phys. Rev. Lett.* 2012, **108**, 156403.
19. C. G. Van de Walle, A. Janotti, *Phys. Status Solidi B*, 2011, **248**, 19.
20. W. Kohn, L.J. Sham, *Phys. Rev.*, 1965, **140**, A1133.
21. G. Kresse, J. Hafner, *Phys. Rev. B*, 1993, **47**, 558.
22. H.J. Monkhorst, J.D. Pack, *Phys. Rev. B*, 1976, **13**, 5188.
23. J. Zheng, G. Ceder, T. Maxisch, W. K. Chim, and W. K. Choi, *Phys. Rev. B*, 2006, **73**, 104101.

24. J.P. Perdew, J.A. Chevary, S.H. Vosko, K.A. Jackson, M.R. Pederson, D.J. Singh, C. Fiolhais, Phys. Rev. B, 1992, **46**, 6671-6687.
25. J.P. Perdew, K. Burke, M. Ernzerhof, Phys. Rev. Lett., 1996, **77** 3865.
26. J.P. Perdew, K. Burke, M. Ernzerhof, Phys. Rev. Lett., 1997, **78** 1396.
27. S. L. Dudarev, G. A. Botton, S. Y. Savrasov, C. J. Humphreys, and A. P. Sutton, Phys. Rev. B 1988, **57**, 1505.
28. F. Furche, Phys. Rev. B 2001, **64**, 195120
29. A. S. Kaygorodov, V. V. Ivanov, V. R. Khrustov, Yu. A. Kotov, A. I. Medvedev, V. V. Osipov, M. G. Ivanov, A. N. Orlov, A. M. Murzakaev, J. Eur. Cera. Soc. 2007, **27**, 1165.
30. D. R. Stull and H. Prophet, JANAF Thermochemical Tables, Natl. Bur. Stan. (U.S.), 2nd ed. Washington, DC: U.S. GPO, 1971.
31. K. K. Kelley, Contributions to Data on Theoretical Metallurgy: Y, Heats of Fusion of Inorganic Substances, U.S. Bur. Mines Bull., No. 393, 166 pp. (1936)
32. C. R. Stanek, K. J. McClellan, M. R. Levy, and R. W. Grimes, IEEE Trans. Nuc. Sci. 2008, **55**, 1492.
33. A. Baldereschi, S. Baroni, and R. Resta, Phys. Rev. Lett. 1988, **61**, 734.
34. F. Réal, V. Vallet, J. P. Flament, and J. Schamps, J. Chem. Phys. 2007, **127**, 104705.
35. M. Peressi, N. Binggeli, and A. Baldereschi, J. Phys. D 1988, **31**, 1273.
36. L. Schmidt-Mende and J. L. Macmanus-Driscoll, Mater. Today 2007, **10**, 40.

Affiliations

^aCenter for Computational Science, Korea Institute of Science and Technology, Hwarangro 14 Gil 5, 136-791, Seoul, Korea. Fax: +82 2 958 5451; Tel: + 82 2 958 5491; E-mail: sckim@kist.re.kr

^bCenter for Materials Architecturing, Korea Institute of Science and Technology, Hwarangro 14 Gil 5, 136-791, Seoul, Korea.

<Graphical Abstract>

